



# Thermal and maturation history for Carboniferous source rocks in the Junggar Basin, Northwest China: implications for hydrocarbon exploration

Di Hu<sup>1,2,3</sup> · Song Rao<sup>4</sup> · Zhu-Ting Wang<sup>1,2,3</sup> · Sheng-Biao Hu<sup>1,2,3</sup>

Received: 9 April 2019 / Published online: 6 January 2020  
© The Author(s) 2020

## Abstract

The reconstruction of thermal history is an important component of basin evolution and hydrocarbon exploration. Based on vitrinite reflectance data, we integrate the paleo-temperature gradient and paleo-heat flow methods to reconstruct the thermal history of Junggar Basin. Compared with present thermal state, the Junggar Basin experienced much a higher heat flow of ca. 80–120 mW/m<sup>2</sup> during the Carboniferous. This feature can be attributed to large-scale volcanic events and related thermal effects. The hydrocarbon maturation history of Carboniferous source rocks indicates that the temperature rapidly reached the threshold of hydrocarbon generation during the Late Carboniferous and has never achieved such a high level since then. This characteristic resulted in the early maturation of hydrocarbons in Carboniferous source rocks. Meanwhile, the results reveal that hydrocarbon maturities are different among various tectonic units in Junggar Basin. The kerogen either rapidly broke through the dry gas period so that cracking of gas occurred or remained in the oil maturation window forming oil reservoirs, which depended on the tectonic background and depositional environment. In this study, we present the thermal and hydrocarbon maturation history since the Carboniferous, which has important implications for further hydrocarbon exploration in Junggar Basin.

**Keywords** Thermal history · Hydrocarbon maturation modeling · Vitrinite reflectance · Carboniferous · Source rocks · Junggar Basin

---

Edited by Jie Hao

**Electronic supplementary material** The online version of this article (<https://doi.org/10.1007/s12182-019-00392-2>) contains supplementary material, which is available to authorized users.

---

✉ Song Rao  
raosongyu@126.com

- <sup>1</sup> State Key Laboratory of Lithospheric Evolution, Institute of Geology and Geophysics, Chinese Academy of Sciences, Beijing 100029, China
- <sup>2</sup> University of Chinese Academy of Sciences, Beijing 100049, China
- <sup>3</sup> Innovation Academy for Earth Science, Chinese Academy of Sciences, Beijing 100029, China
- <sup>4</sup> Key Laboratory of Exploration Technologies for Oil and Gas Resources, Ministry of Education, Yangtze University, Wuhan 430100, Hubei, China

## 1 Introduction

With the growing demand for hydrocarbon resources and the deepening of exploration activities, the target stratigraphy for present oil and gas exploration has been shifted to the deep (> 4500 m) and ultra-deep zones (Sun et al. 2013; Zhao et al. 2013), which are currently important strategic areas for hydrocarbon prospecting and exploitation (He et al. 2016). The Junggar Basin is one of the largest oil and gas basins in western China and is characterized by a thickened basement crust, low geothermal gradient, and widespread deep-seated strata (Pan et al. 1997; Qiu et al. 2008; Rao et al. 2013; Wang et al. 2001; Zhang et al. 2007). During recent decades, several deep Carboniferous oil and gas fields such as the Wucaiwan, Shixi, and Karameli gas fields have been discovered and exploited, which bodes well for the deep zone of the Junggar Basin (He et al. 2010; Li et al. 2009). The thermal evolution of basin is closely linked to the generation, migration, accumulation, and preservation of hydrocarbons in the traps combined with the burial history (Mashhadi

et al. 2015). Hence, thermal evolution of the source rock is related to evaluate the petroleum prospectivity in the basin.

The Junggar Basin is a multi-cycle superimposed basin and has experienced multi-stage tectono-thermal evolution since the Late Carboniferous. Previous researchers have conducted many studies on the thermal regime of the Junggar Basin and the evolution of the Carboniferous source rocks. The results could be summarized as follows: (1) the high geothermal gradient gradually decreased from the Carboniferous to the Cenozoic (Pan et al. 1997; Qiu et al. 2005; Wang et al. 2001); (2) the source rocks evolved early due to the high geothermal effect during the Late Paleozoic (Cao et al. 2005; Qiu et al. 2005); and (3) Carboniferous pyroclastic rocks formed by large-scale volcanic activity are not only effective source rocks but also provide favorable reservoir conditions for later oil and gas accumulation (He et al. 2010). However, previous studies have mainly focused on the thermal history since the Permian, and only an approximate estimate of the thermal state has been provided during the Carboniferous. Meanwhile, the main controlling factors of thermal evolution and their relations with regional tectonic events have not been properly evaluated. There is also a little understanding of the hydrocarbon maturation period of Carboniferous source rocks in Junggar Basin.

In this study, the 1D reconstruction of thermal history recorded by considerable vitrinite reflectance ( $R_o$ ) data from wells LN-1, MS-1, CS-2 and Ca-6, utilizing the paleo-geothermal gradient and paleo-heat flow methods. Moreover, we precisely simulate the thermal history and hydrocarbon maturation history of the Junggar Basin since the Late Carboniferous by the basin modeling, and the thermal maturity stage of the Carboniferous source rock is established under the constraints of the regional geodynamic background. We also discussed the genesis of locally high heat flow in the Carboniferous and the potential of the Carboniferous hydrocarbon system. The thermal and maturation history will help to understand the tectonic evolution during Carboniferous and have important implications for further hydrocarbon exploration in Junggar Basin.

## 2 Geological background

The Junggar Terrane, which is near the northwestern margin of China and is tectonically a part of the Central Asian Orogenic Belt, consists of the West Junggar Terrane, the East Junggar Terrane and the Junggar Basin (Fig. 1a) (Han et al. 2010; Li et al. 2016; Şengör et al. 1993; Xiao et al. 2008). The Junggar Basin is bounded by the Tianshan Mountains on the south and the Altai Mountains on the north (Fig. 1b), with an area of approximately  $13 \times 10^4 \text{ km}^2$  (Ma et al. 2018). The West Junggar Terrane and East Junggar Terrane are mainly fold-thrust orogenic belts composed of Paleozoic

accretionary complexes, volcanic arcs and high-grade metamorphic ophiolite zones (Xiao et al. 2008, 2011; Zhang et al. 2009). The NE West Junggar folded orogenic belt is a suture zone where the Junggar Terrane collided with the Kazakhstan plate. The East Junggar Terrane was formed during the northward subduction of the southern Paleo-Asian Ocean, and the North Tianshan fold orogenic belt might be a collision product between the Junggar plate and the Tarim Block (Li et al. 2015, 2016; Xiao et al. 2011).

### 2.1 Basin evolution

The Junggar Basin is a superimposed basin that has developed since the Late Carboniferous; Xiao et al. (2008) concluded that the basement of the Junggar Basin is mainly composed of volcanic arcs, accretionary complexes and trapped residual oceanic crust from the Paleozoic. He et al. (2013) determined that the SHRIMP U–Pb age of a Carboniferous andesitic tuff in the MS-1 well is  $331.7 \pm 3.8 \text{ Ma}$ ; thus, the Early Carboniferous is a crucial period from the closing of the Junggar Ocean to the rapid growth of new continental crust based on Hf isotope analysis (Zhang et al. 2007). A number of unconformities and tectonic layers were formed after multiple periods of tectonic movement corresponding to the rifting stage from Late Carboniferous to Permian (Carroll et al. 2010), the Triassic–Paleogene intracratonic depression stage (Jolivet et al. 2010) and the rejuvenated foreland basin stage since the Neogene (Fig. 2). The Junggar Basin is generally subdivided into six first-order tectonic units according to the basic structural characteristics (Fig. 1c; I–VI, respectively): Wulungu Depression, Luliang Uplift, Western Uplift, Central Depression, Eastern Uplift and Southern Depression.

### 2.2 Sedimentary strata

The sedimentary cover of the Junggar Basin is well developed, and the depositional thickness can be up to 15,000 m locally (Fig. 3). The Carboniferous, Permian, Triassic, Jurassic, Cretaceous and Cenozoic systems from bottom to top are overlapped on top of pre-Carboniferous volcanic and metamorphic rocks (Cai 2009; Yang et al. 2012b). A transitional facies sedimentary system accompanied by intermittent volcanic eruptions is recorded by Late Paleozoic sediments, whereas a set of clastic sediments of Mesozoic and Cenozoic ages reveals continental facies.

The Carboniferous is a critical period for the cratonization of the Junggar terrane, when two continental passive margins were developed on the southern and northern margins, and thick volcanoclastic rocks (Fig. 3) filled in the rifts (He et al. 2010). The Carboniferous strata in the Junggar Basin mainly deposited as marine–terrestrial alternating facies (Li et al. 2009). Only low-grade metamorphic sandstone,

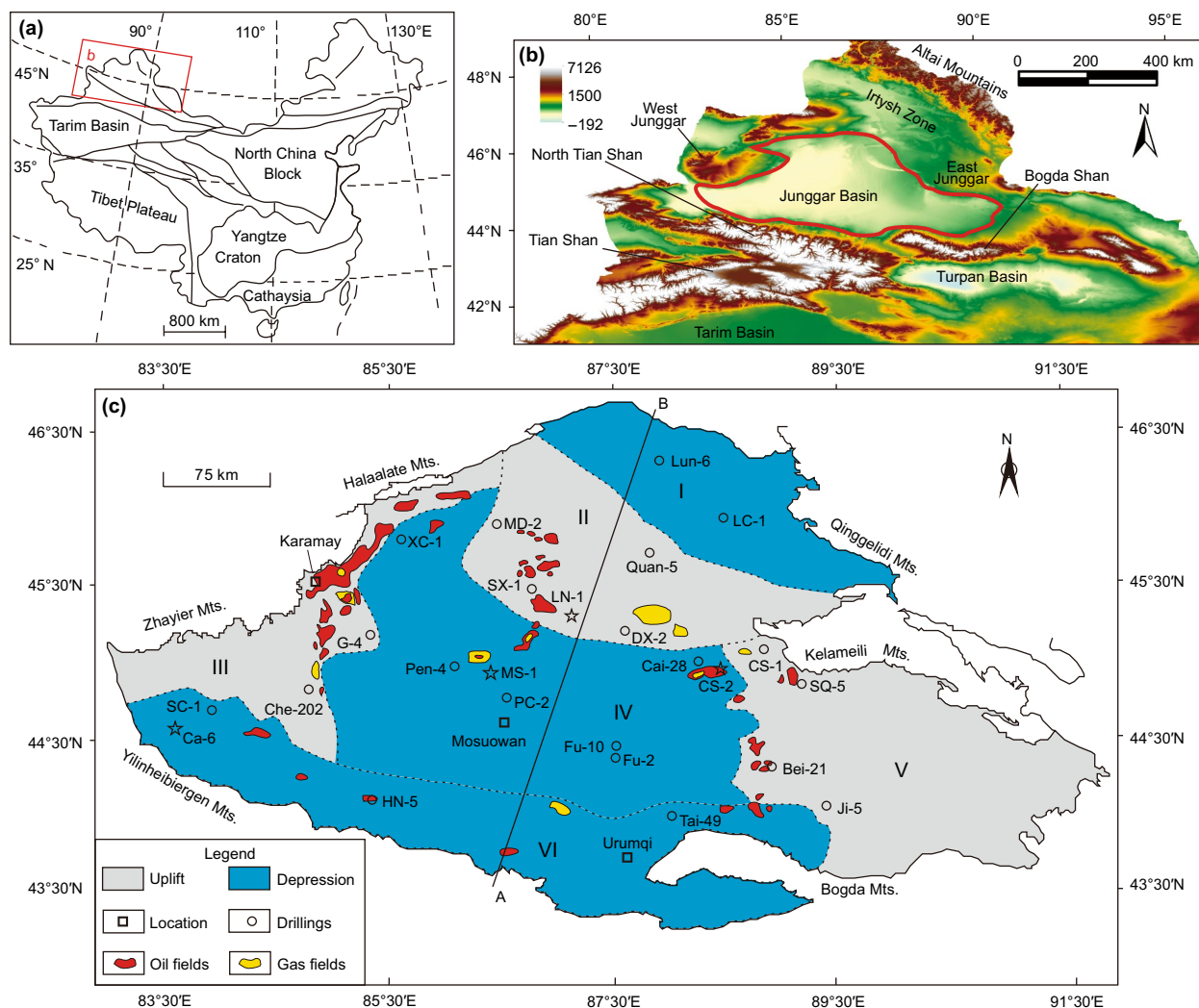


**Fig. 1** **a** Locations of the Junggar Terrane, Tarim Basin, North China Block and Tibetan Plateau. **b** Peripheral elevation topographic map and mountains of the Junggar Basin. **c** Structural unit map showing the locations of oil and gas fields and typical drillings in the Junggar Basin (modified from He et al. 2010). I. Wulungu Depression; II. Luliang Uplift; III. Western Uplift; IV. Central Depression; V. Eastern Uplift; VI. Southern Depression; Mts. = Mountains. The stars represent the location of modeled drillings

slate, siliceous slate and intermediate acid volcanics of the Lower Carboniferous ( $C_1$ ) occur in the Altai region, whereas abundant sandstone, siltstone, tuff and volcanic rocks of the Lower to Upper Carboniferous ( $C_1$ – $C_2$ ) are widespread in other regions (Han et al. 2010; He et al. 2013; Jin et al. 2008; Yang et al. 2012b). Meanwhile, many recent chronological studies on Carboniferous strata yield U–Pb ages of zircons from  $350.0 \pm 6.3$  to  $299.8 \pm 5.2$  Ma based on different lithologies, including rhyolite, basalt, tuff and andesite (Tan et al. 2009; Yang et al. 2012b).

### 2.3 Carboniferous source rocks

Multiple depocenters were formed during the Carboniferous in the Junggar Basin, and the volcanoclastic rocks can be

up to 2.0–5.0 km in thickness (He et al. 2010). The Dishuiquan Formation ( $C_1d$ ) and Batamay Formation ( $C_2b$ ) occur within or around the basin, and the thickness of effective source rocks can reach 400–800 m. The Carboniferous source rocks included organic-rich gray mudstone, tuffaceous mudstone, silty mudstone and tuffs, which primarily deposited in marine–terrestrial environment containing type II–III kerogen (Wang et al. 2013). The total organic carbon (TOC) value of Carboniferous source rocks changed dramatically and indicated great oil generation potential. Typically, the mudstones have TOC values with the average of 1.45%; carbonaceous with the average of 15.53%; coals with the average of 43.78%; tuffs with the average of 1.56% (Li et al. 2009). Maturity of the Carboniferous source rocks is generally high with vitrinite reflectance ( $R_o$ ), and the details

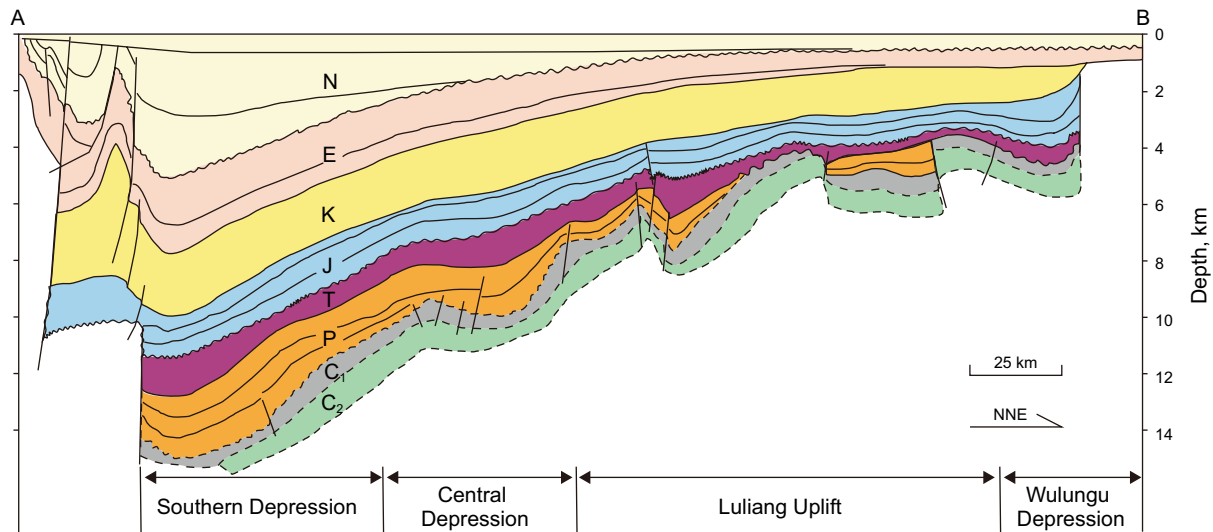


**Fig. 2** South–north geological transect across the Southern Depression, Central Depression, Luliang Uplift and Wulungu Depression (modified from Yang et al. 2012a). The thicknesses of Carboniferous strata are estimated according to new drilling data. The location of profile A–B is shown in Fig. 1

will be described in next chapter. Hence, the Carboniferous source rocks are mainly in high-post mature stage. The oil correlation results of Carboniferous source rocks suggest that the oil from volcanic reservoir rocks within the  $C_2b$  Formation generally correlates with the  $C_1d$  source rocks based on molecular and carbon isotopic data (Yu et al. 2014). However, a small amount of younger source rocks from the Middle Permian and Lower Jurassic also can feed to the Carboniferous reservoirs in some regions (Yu et al. 2014). Overall, these source rocks could provide effective supplies of oil and gas for the Carboniferous pyroclastic and the Permian clastic reservoirs (He et al. 2010; Li et al. 2009; Wang et al. 2010).

## 2.4 Carboniferous reservoir

The discovered Carboniferous hydrocarbons mainly reserved on the volcanic rocks of Batamay Formation ( $C_2b$ ) by now, although the sandy conglomerates of Lower Carboniferous could be potential reservoir. The Batamay Formation ( $C_2b$ ) contains grayish green basalts, andesites, tuffs with minor gray sandstones, dark gray mudstones, carbonaceous mudstones and coals (Wang et al. 2010). These volcanic rocks could form the weathering crust and the interior interval reservoirs with favorable porosity and permeability condition owing to the long periods of weathering and leaching, the dissolution of organic acid or deep thermal fluids (He et al. 2010). Except for regional mudstone seal from Triassic or Permian, the thick source rocks of Batamay Formation ( $C_2b$ ) also could be good seal to form self-generated and self-stored reservoir.

## 3 Methodology and data

The thermal stage of a basin plays an important role not only in regional tectonic evolution but also in controlling the generation, migration, accumulation and preservation of oil and gas (Hudson and Hanson 2010). The principles for the reconstruction of the thermal history of a sedimentary basin can be summarized as follows:

1. On the lithospheric scale, the heat flow history of the basin can be determined by a mathematical and geophysical model, depending on the geodynamic mechanism of the basin and the heat transfer pattern from the Earth's interior. Through adjusting the parameters of model, the modeled results are accordance with observed temperature and subsidence characteristics.
2. On the basin scale, the thermal history can be quantitatively recovered through types of indicators recording paleo-temperature information (Chang et al. 2016, 2018; Sweeney and Burnham 1990). The modeling methods fall into three categories: the stochastic inversion of a single sample, the paleo-geothermal gradient method based on a vertical profile and the paleo-heat flow method based on a suite of downhole samples (Lerche et al. 1984; Tang et al. 2014).

### 3.1 Inversion method

Considering the complex geological background of the Junggar Basin, the paleo-geothermal gradient and the paleo-heat flow methods (Lerche et al. 1984; Wang et al. 2001) are

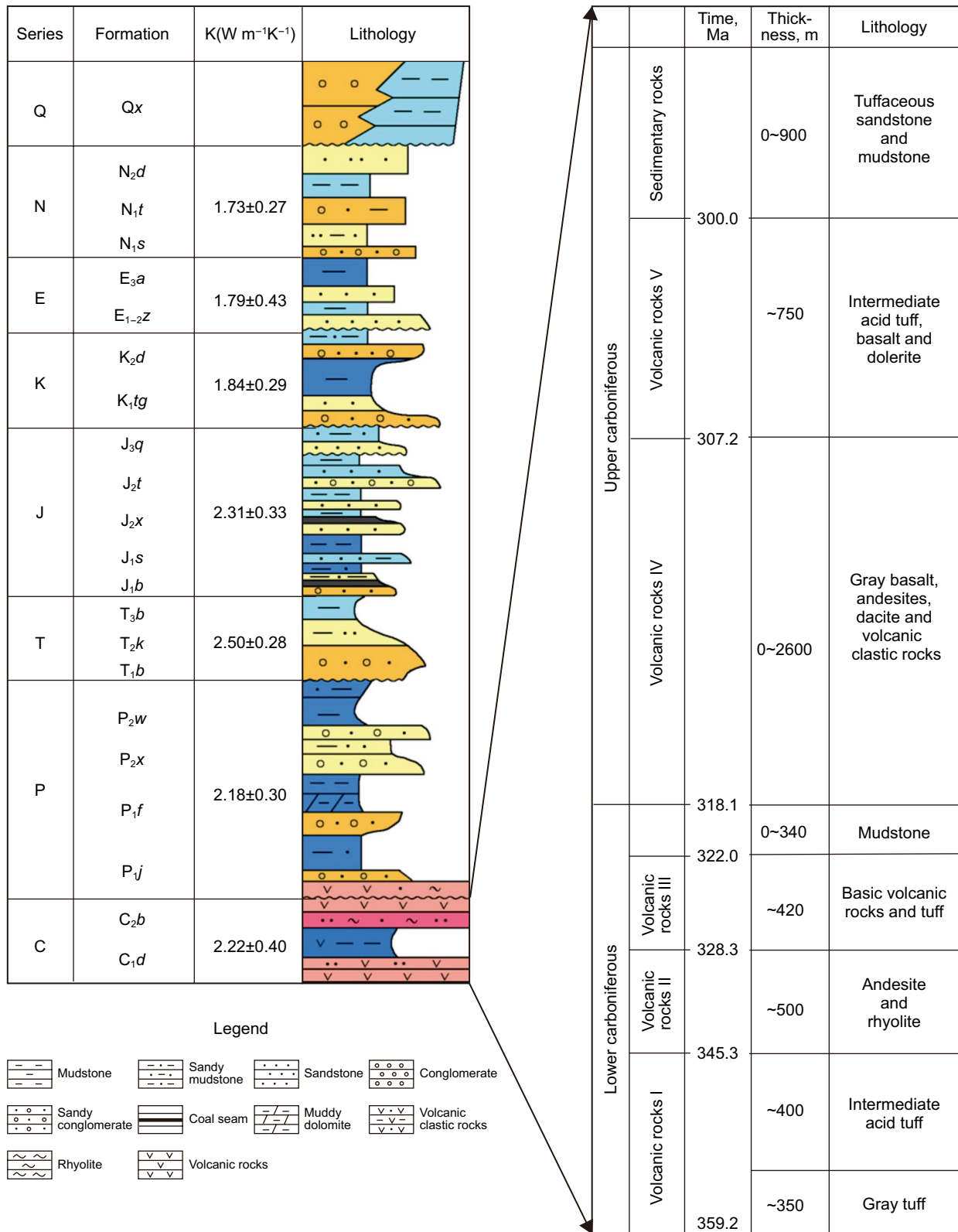


**Fig. 3** Comprehensive stratigraphic column and details of Carboniferous volcanic strata in the Junggar Basin (modified from Wang et al. 2010). Thermal conductivity values (*K*) are from Rao et al. 2013, which are used for later thermal modeling



integrated to reconstruct the thermal history. We use the paleo-geothermal gradient method to define the thermal history before reaching the maximum paleo-temperature and invert the uncertain thermal history through various heat flow paths coupled with the burial history. The best-fit path coinciding with thermal indicator data is selected as the final result. Inversion modeling is performed by the software Thermodel (Hu et al. 2001) constrained by a heat conduction and compaction model. Present geothermal gradients, present heat flow, thermal conductivity and heat production data are from Rao et al. (2013), while other related parameters such as the compacting factor and porosity are adopted according to the software default values.

### 3.2 Thermal indicators

Considering the lack of fission track data in the Junggar Basin (Qiu et al. 2005; Wang et al. 2001), we mainly utilize vitrinite reflectance as the thermal indicator. Vitrinite reflectance ( $R_o$ ) is one of the most popular thermal maturity indices to measure experienced maximum temperature of organic matter. Each  $R_o$  value can be translated to a maximum paleo-temperature value using the EASY%  $R_o$  chemical kinetics model (Sweeney and Burnham 1990). For this paper, 633  $R_o$  data were systematically collected from 30 drillings, mainly collected from the PetroChina Xinjiang Oilfield Company. The histogram distributions of  $R_o$  data are drawn for the Jurassic, Triassic, Permian and Carboniferous (Fig. 4), and the detailed results of  $R_o$  are shown in the supplementary material.

The relatively low average  $R_o$  values of Jurassic and Triassic Formations indicate their low-mature organic matter and are consistent with the low thermal background since the Mesozoic (Cao et al. 2005; Qiu et al. 2008). However, Carboniferous  $R_o$  values show a wider distribution and relatively high thermal maturity. Meantime, the differences in frequency distributions of  $R_o$  values between Late Paleozoic and Meso-Cenozoic rocks indicate completely different thermal regimes. The difference of current maturity in the Carboniferous source rocks is clear and may show a change from low maturity to high maturity. For example, the  $R_o$  values of the Dishuiquan group ( $C_1d$ ) range from 0.56% to 0.63% in well Cai-28, 1.69%–1.76% in well LN-1 and 1.13%–4.15% in well MS-1 (Fig. 1c). The Batamay group samples ( $C_2b$ ) in the northwestern basin have moderate maturity with  $R_o$  between 0.86% and 1.18%, mainly in oil maturation window, whereas it reaches the overmature phase in other regions (He et al. 2010). Four representative vitrinite profiles show that there is a  $R_o$  “jump” or “break” phenomenon at the disconformity due to uplift and erosion of underlying strata or changing of the geothermal gradient, which establishes

the foundation for quantitative reconstruction of the thermal history of the region.

## 4 Results

### 4.1 Thermal history of well LN-1

The simulated results of well LN-1 located in the Luliang uplift are presented (Fig. 1c, II) to introduce the specific reconstruction procedure. The Formations and lithology in well LN-1 are shown in Table 1. The well was drilled from the Oligocene unit to the Carboniferous unit with a total depth of 4905.5 m.

Firstly, the paleo-geothermal gradient method is utilized to acquire the maximum paleo-geothermal gradient and erosion thickness in mainly unconformities. There are several unconformities or disconformities observed in well LN-1, but two are major: the absence of the Upper Carboniferous to Middle Permian and of the Neogene to present units. Thus, the sedimentary strata (Table 1) can be approximately divided into two subsections: Paleogene to Permian (subsection I) and Carboniferous (subsection II). The paleo-temperature profiles are measured by the  $R_o$  data of different layers (Fig. 5a). The paleo-temperature gradient ( $dT/dz$ ) for each subsection can be obtained using a linear least-squares fit according to the paleo-temperature profile (Fig. 5b). The eroded thickness is calculated by dividing the difference between the surface temperature ( $T_s$ ) and the intercept of the paleo-temperature profiles ( $T_i$ ) at the top unconformity by the estimated paleo-temperature gradient using the equation:  $E_i = (T_i - T_s)/(dT/dz)_i$  (where  $i$  represents the code of each subsection). The results indicate that the paleo-temperature gradient and erosion thickness of subsection II reach 44.9 °C/km and 2550 m, respectively, and 26.5 °C/km and 300 m, respectively, for subsection I (Fig. 5c, d). Meanwhile, the paleo-heat flow of well LN-1 decreases from 95.8 mW/m<sup>2</sup> in the Late Carboniferous to 54.2 mW/m<sup>2</sup> at the end of the Late Paleogene (Fig. 5d).

Further, the reasonable paleo-heat flow results and eroded thickness defined by the paleo-geothermal gradient method are imported into the software Thermodel. Then, we can screen the best-fit eroded thickness ( $H_e$ ) and paleo-heat flow ( $Q$ ) through multiple iterations. The detailed burial and thermal history (Fig. 6a, c) show that both a high deposition rate (80 m/Ma) and high heat flow (–100 mW/m<sup>2</sup>) occurred in the Early Carboniferous. The heat flow gradually decreased to approximately 80 mW/m<sup>2</sup> in the Early Triassic along with a rapid erosion event, followed by a relatively stable depositional period since the

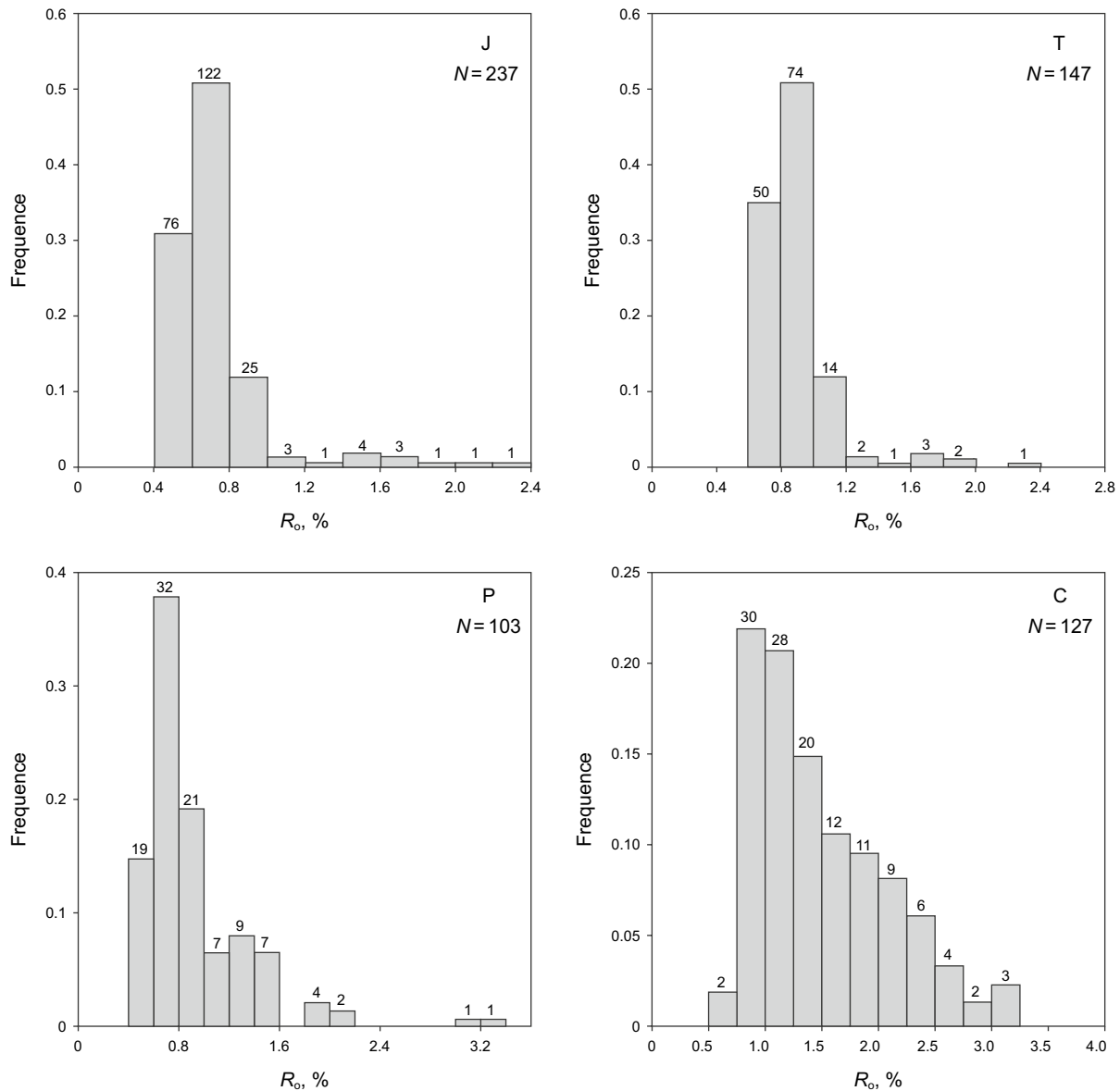


**Fig. 4** Histogram distribution of  $R_o$  in the Junggar Basin. Data from the Petro China Xinjiang Oilfield Company

Late Triassic. The heat flow was approximately  $50 \text{ mW/m}^2$  in the Late Cretaceous, which is close to the present level. Figure 6b verifies the reliability of the inversion results through comparing the modeled  $R_o$  values with measured  $R_o$  values.

#### 4.2 Thermal characteristics of the Junggar Basin

For superimposed basins, the thermal history recorded by various wells should be jointly analyzed to form an integrated complete thermal sequence. Therefore, we reconstruct

the thermal history (Fig. 7) of 3 other wells in the Junggar Basin, including MS-1 (III, Central Depression), CS-2 (VI, Eastern Uplift) and Ca-6 (V, Southern Depression) (Fig. 1c). Well MS-1 is in the Central Depression and has a drilling depth of 7500 m, which is one of the deepest wells in the Junggar Basin. The reconstructed thermal history of the Central Depression is characterized by high paleo-heat flow ( $> 120 \text{ mW/m}^2$ ) in the Carboniferous, followed by rapid uplift and erosion from 290 to 260 Ma (Fig. 6a). The eroded thickness is close to 4.0 km, and the heat flow decreases to approximately  $85 \text{ mW/m}^2$  during this stage. A similar

**Table 1** Formations and lithology of well LN-1

Group	Code	Bottom, m	Thickness, m	Lithology
Anhe	E <sub>3a</sub>	760	760	Gray gravel layer and clay bed
Ziniquan	E <sub>1+2z</sub>	1154	394	Gray silty mudstone and brown coarse-grained sandstone
Donggou	K <sub>2d</sub>	1390	236	Brown red sandy mudstone and red siltstone
Tulufan	K <sub>1tg</sub>	3044	1654	Brown mudstone and fine sandstone
Xishanyao	J <sub>2x</sub>	3164	120	Gray green mudstone and gray conglomerate with coal seam
Sangonghe	J <sub>1s</sub>	3381	217	Dark gray mudstone and dark gray silty mudstone
Badaowan	J <sub>1b</sub>	3853	472	Green gray conglomerate with black coal seam
Baijiantan	T <sub>3b</sub>	4044	191	Gray green mudstone and gray sandstone
Karamay	T <sub>2k</sub>	4170	126	Brown gray silty mudstone and fine sandstone
Baikouquan	T <sub>1b</sub>	4307	137	Dark gray green tuffaceous sandstone and conglomerate
Wuerhe	P <sub>2w</sub>	4571	264	Gray black carbonaceous mudstone and sandy conglomerate
Batamay	C <sub>2b</sub>	4905.5	334.5↓	Green gray andesite, brown gray tuff and gray rhyolite

decrease in heat flow occurs in three other wells LN-1 (4905.5 m), CS-2 (3752.0 m) and Ca-6 (4430.0 m) from approximately 100 mW/m<sup>2</sup> in the Carboniferous to 50 mW/m<sup>2</sup> at present. It is worth mentioning that well LN-1 and CS-2 show a small-amplitude continued uplift process in the Late Paleogene.

In general, the Junggar Basin has experienced constantly decreasing heat flow since the Late Carboniferous. The reconstructed thermal histories of all modeled wells indicate paleo-heat flows of 80–100 mW/m<sup>2</sup> from the Late Carboniferous to Early Permian, decreasing to the present level of 40–50 mW/m<sup>2</sup>. The heat flow evolution of the tectonic units in the basin shows lateral heterogeneity. During the Carboniferous, the highest heat flow of the basin was in the Eastern Uplift, but during the Permian, the Central Depression showed the highest heat flow value, while the heat flow of the southern part of the basin always maintained a relatively low level. The heat flow distribution of the entire basin has been consistent with the present since the Triassic.

Previous researchers mainly focused on thermal history and eroded events after Permian (Wang et al. 2013). Li et al. (2009) and Qiu et al. (2005) consider the eroded thickness at about 0.5–1.5 km between late Carboniferous to early Permian in Central Depression, and these results are reasonable in the Wucuiwan and Dongdaohaizi sag. Our burial history indicates that the eroded thickness could be reach to 2.0–4.0 km since late Carboniferous because these drillings are located in uplift region (Fig. 1c). Well Ca-6 even reveals the unconformity between late Carboniferous and Jurassic in the North Tianshan Thrust Belt.

### 4.3 Thermal maturity history

The thermal evolution of source rocks refers to the maturity state of source rocks in different geological periods and is an important part to evaluating hydrocarbon generation. Based on the reconstruction of the burial and heat flow history (Fig. 7), we can acquire the temperatures of hydrocarbon source rocks at various stages. Furthermore, the  $R_o$  vs time curves can be estimated to infer the maturity of source rocks according to the thermal paths and the EASY%  $R_o$  chemical kinetics model (Sweeney and Burnham 1990).

The geothermal and maturity histories of the CS-2 well (Fig. 8) show that the burial depth of the Lower Carboniferous (C<sub>1</sub>) was only approximately 1200 m, but the temperature had already reached more than 90 °C by 320 Ma, which broke through the oil maturation threshold and quickly reached the oil window peak. The C<sub>1</sub> strata reached their highest temperature of approximately 150 °C in the Late Carboniferous and entered the late oil window period. Since then, the temperature of the C<sub>1</sub> has never been more than 150 °C due to later erosion and decreasing thermal background. Hence, the Lower Carboniferous source rocks of well CS-2 matured rapidly during the Late Carboniferous–Early Permian and have remained in the late oil window period since ca. 250 Ma (Fig. 8). Meanwhile, the results indicate that the hydrocarbon maturation history is very different among various tectonic units in the Junggar Basin (Fig. 9). The  $R_o$  of Carboniferous strata in well MS-1 has been close to 4.0% during geological time, corresponding to the overmaturity



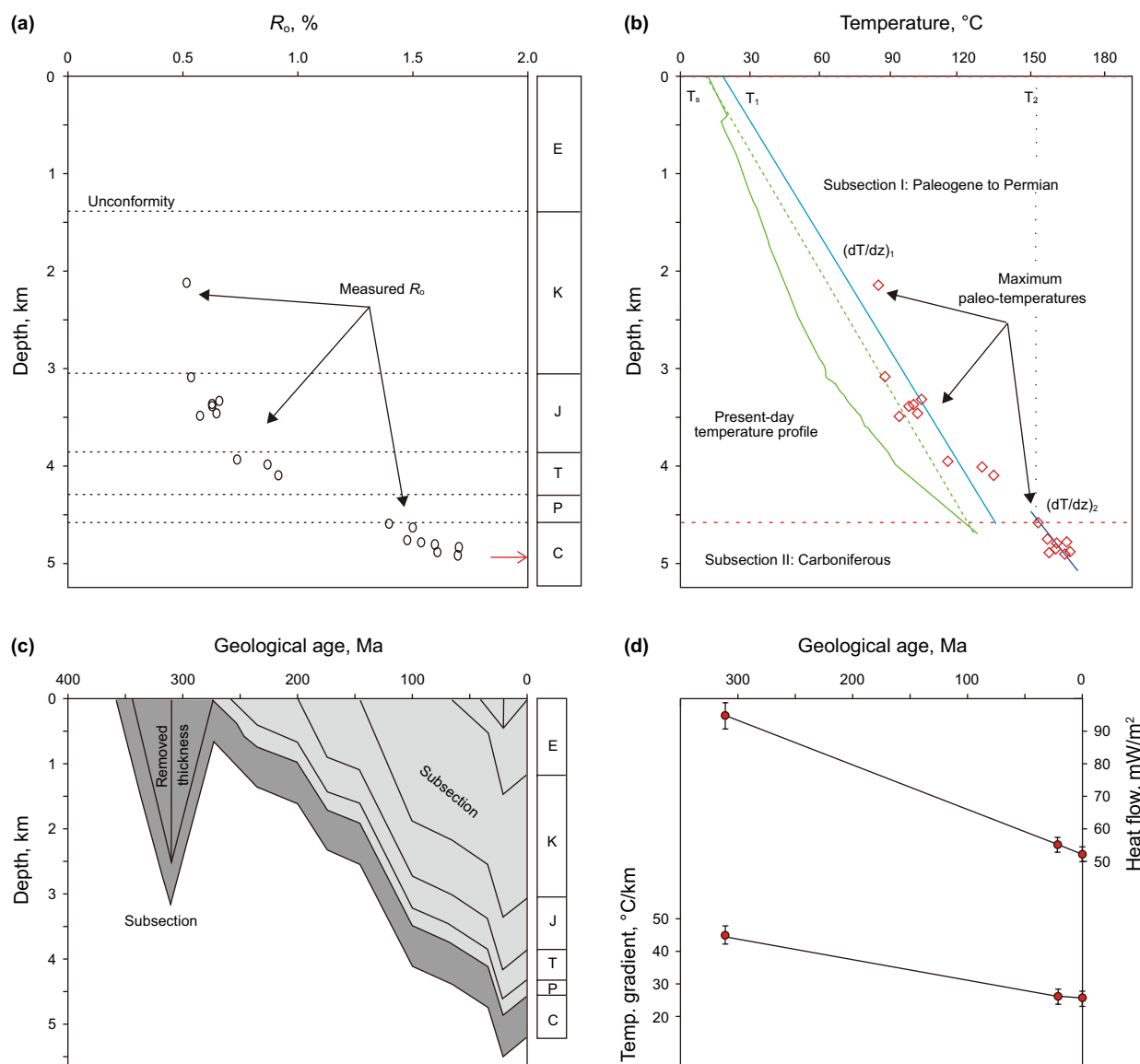


**Fig. 5** Modeling results based on paleo-temperature gradient generated from  $R_o$  profile of well LN-1 in Luliang Uplift. **a** Measured  $R_o$  profile and unconformities in well LN-1. **b** Maximum paleo-temperature profile measured and fitted by  $R_o$  data using the Sweeney and Burnham (1990) model. Surface temperature ( $T_s$ ) and present-day temperature profile are from Wang et al. 2001. **c** Approximate burial history of well LN-1. **d** Modeled paleo-temperature gradient and heat flow from well LN-1. The error bars represent error ranges of  $\pm 10\%$

phase, whereas the Carboniferous source rocks of well Ca-6 have merely remained at the early oil stage with  $R_o$  value of 1.0%.

## 5 Discussion

### 5.1 Genesis of high heat flow in the Carboniferous

The reconstructed thermal history in the Junggar Basin is closely related to the geodynamic background of this region. Previous research and our modelings (Fig. 7) indicate that

the Junggar Basin has high heat flow values with the average greater than 80 mW/m<sup>2</sup> in the Carboniferous (Qiu et al. 2005). The heat flow of some region (Mosuowan swell) even could have reached 100–120 mW/m<sup>2</sup>, which is similar to the heat flow in mid-oceanic ridges and active volcanic areas. These results may be attributed to intense plate tectonic and simultaneous large-scale volcanic activity (Yang et al. 2012a). The Junggar Basin went through an important transition period from subduction and accretion to collision and amalgamation in the Carboniferous (Li et al. 2015; Xiao et al. 2008). Because of the subduction of oceanic crust and the activation of continental crust (Fig. 10b), frequent and

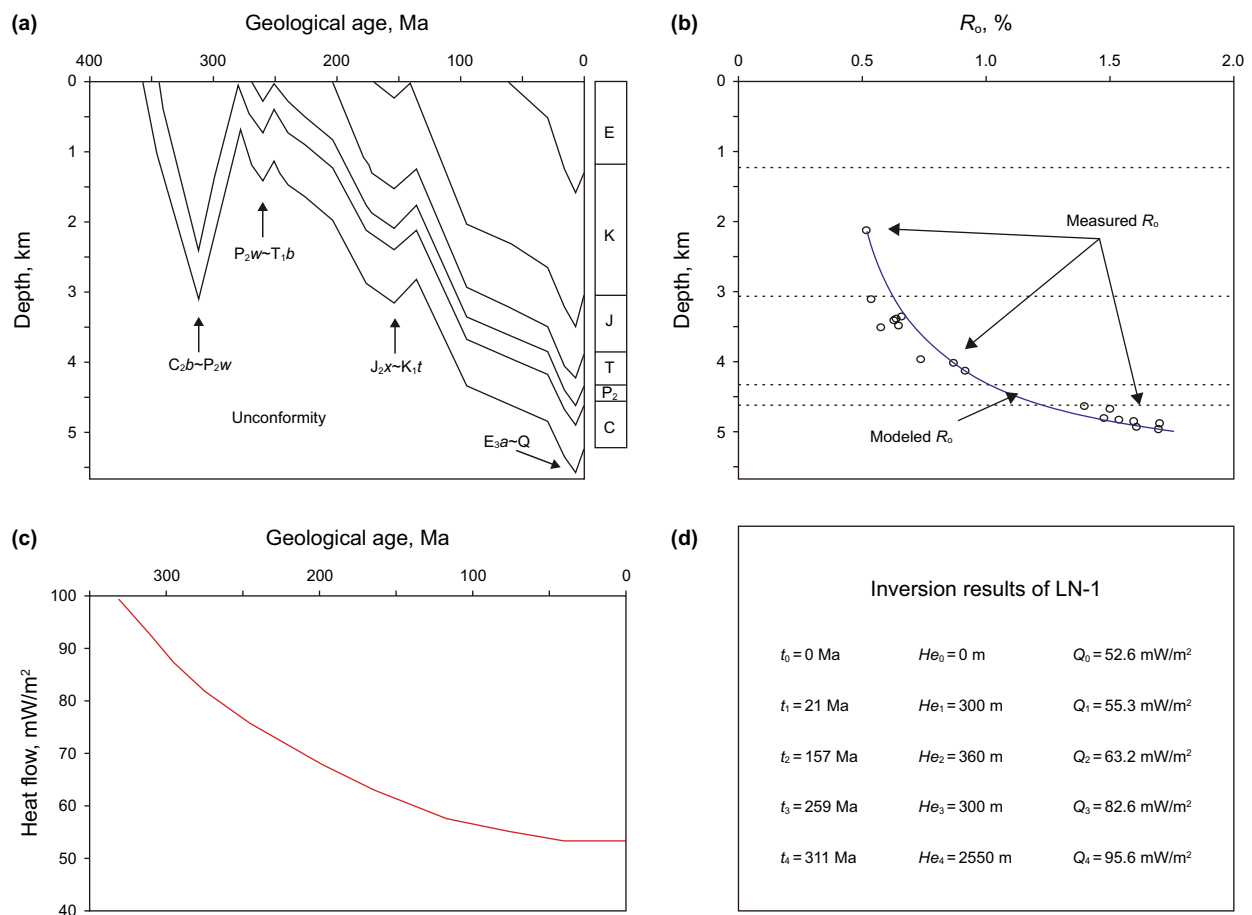


**Fig. 6** Inversion modeling results of well LN-1 based on paleo-heat flow method. **a** Detailed burial history of well LN-1 using software Thermodel (Hu et al. 2001). **b** Consistency between modeled and measured  $R_o$ . The dashed lines represent important discontinuity. **c** Reconstructed paleo-heat flow history. **d** Inversion results of geological time ( $t_i$ ), eroded thickness ( $He_i$ ) and paleo-heat flow values ( $Q_i$ )

large-scale subduction-related volcanic rocks were well developed in the basin as the Junggar Ocean disappeared (Tan et al. 2009; Xiao et al. 2011; Zhang et al. 2009; Zheng et al. 2007).

Figure 10a gives the distribution of Carboniferous volcanic rock, and our modeling wells are located at these volcanic field (He et al. 2010). The age distribution of igneous rocks in the Junggar Basin during the Carboniferous (Fig. 10c) shows that the main peak of igneous events was from 335 to 300 Ma, which indicates that these magma maybe release plenty of heat to form a locally high geothermal gradient field. It is worth to mention that the Tarim Basin is neighbored to the Junggar Basin (Fig. 1a) and has similar thermal history in Paleozoic (Chang et al. 2014, 2017). The Tarim Basin experienced an intracratonic rift from the Middle Carboniferous to the Permian, and the early Permian Large Igneous Province has been systemically studied (Xu et al. 2014). The dramatic magmatic activity could affect the thermal regime of the basins, and the thermal gradient could reach to 30–40 °C/km in the Tarim Basin during

this period (Qiu et al. 2012). This situation is also similar to the thermal regime related to the eruption of the Emeishan Large Igneous Province at 259 Ma in the Sichuan basin (Xu et al. 2001; Zhu et al. 2010).

Furthermore, the rapid uplift and extensive erosion recorded by the unconformity in the Late Carboniferous are coincident with our modeling results (Fig. 7) and are closely related to the compressional tectonic system of the basin that formed in the process of collision (Li et al. 2015, 2016). Hence, we suggest that the high heat flow of the Junggar Basin in Carboniferous could be a result of large-scale volcanic events and related thermal effects.

### 5.2 Hydrocarbon maturation style of Carboniferous source rocks

According to the thermal maturation history of different drillings (Fig. 9), we deduce the hydrocarbon maturation styles of Carboniferous source rocks in the Junggar Basin (Fig. 11). The general hydrocarbon maturation styles can

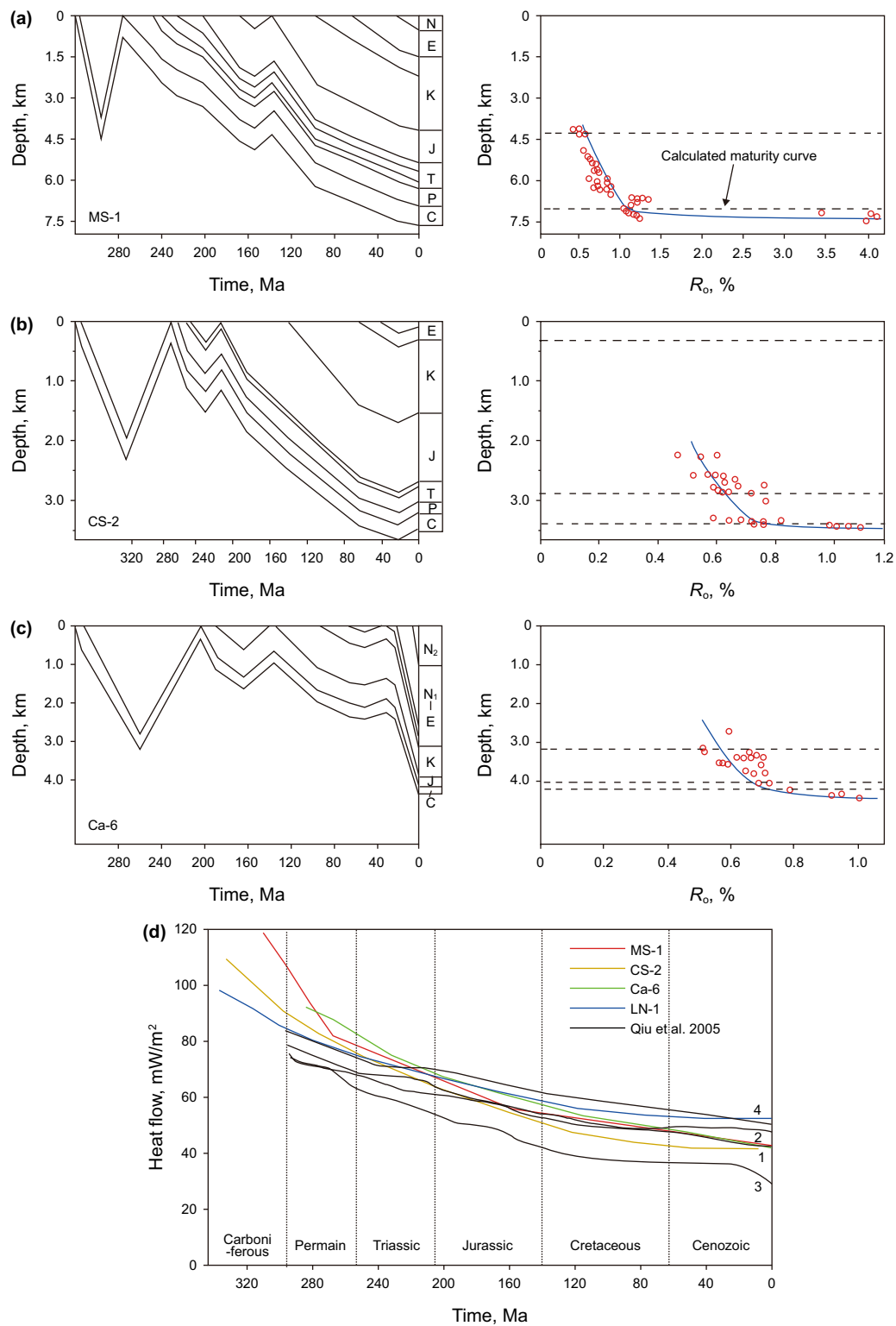


**Fig. 7** Reconstructed thermal history for wells in the Junggar Basin. **a–c** Burial histories and fitting results with vitrinite reflectance of MC-1, CS-2 and K-6 wells, respectively. The blue curves represent calculated maturity, and red dots represent measured  $R_o$  values. The black dashed lines represent important discontinuity. **d** Modeled heat flow histories for studied wells and previous studies (Qiu et al. 2005) 1: Wulungu Depression; 2: Luliang Uplift and Central Depression; 3: Southern Margin; 4: Eastern Uplift area

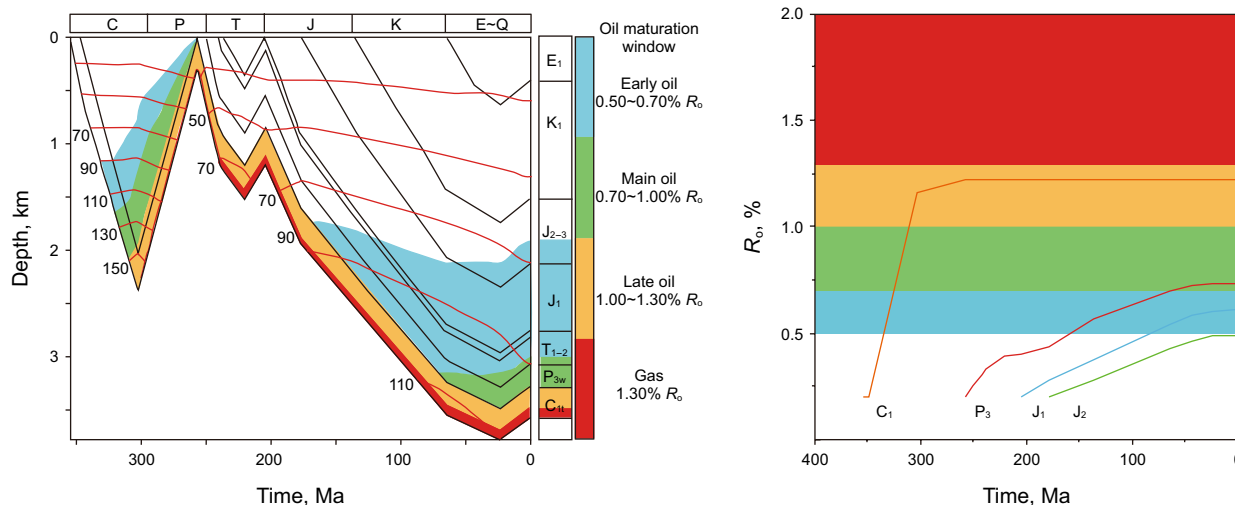


Fig. 8 Geothermal and thermal maturity histories for the CS-2 well

be divided into two types. (1) The kerogens of the Mahu sag (West Uplift) and the Mosuowan swell (Central Depression) passed the threshold of hydrocarbon maturation during the Carboniferous–Permian (the location of these typical sags and swells are showed in Fig. 10a). Then, the kerogens quickly broke through the oil window and the gas window, reaching to the overmature phase with a  $R_o$  value of more than 3.0%. (2) The times of hydrocarbon maturation in the

Wucaiwan sag (East Uplift) and the Sikeshu sag (Southern Depression) started early and simultaneously, but have lower levels of thermal evolution with moderate  $R_o$  at 1.2% and 0.9%, respectively, corresponding to the oil maturation window. These maturation styles mean that both oil and gas fields could have formed in Carboniferous source rocks.

These different styles in maturity may reflect the combined effects of magmatic activity during the Carboniferous Period and the later sedimentary environment in various tectonic positions. As the lithosphere thickened and the supply of mantle heat was reduced, the heat flow has decreased rapidly since the Mesozoic. Considerable sedimentation can also do nothing to help source rocks undergoing higher temperatures (Fig. 2). This high thermal background results in rapid hydrocarbon maturation for Carboniferous source rocks and no higher maturity due to a continuous decrease in heat flow after this time. Meanwhile, the rapid deposition since the Mesozoic can lead to the development of stratigraphic overpressure, which is helpful for the migration and accumulation of oil and gas (Luo et al. 2007). Hence, the Carboniferous Formations preserve conditions for the development of large oil and gas fields in the Junggar Basin from the perspective of thermal evolution.

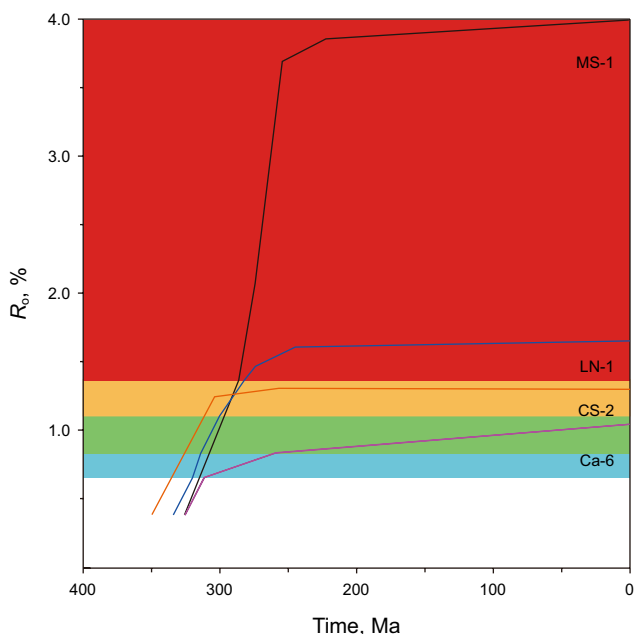
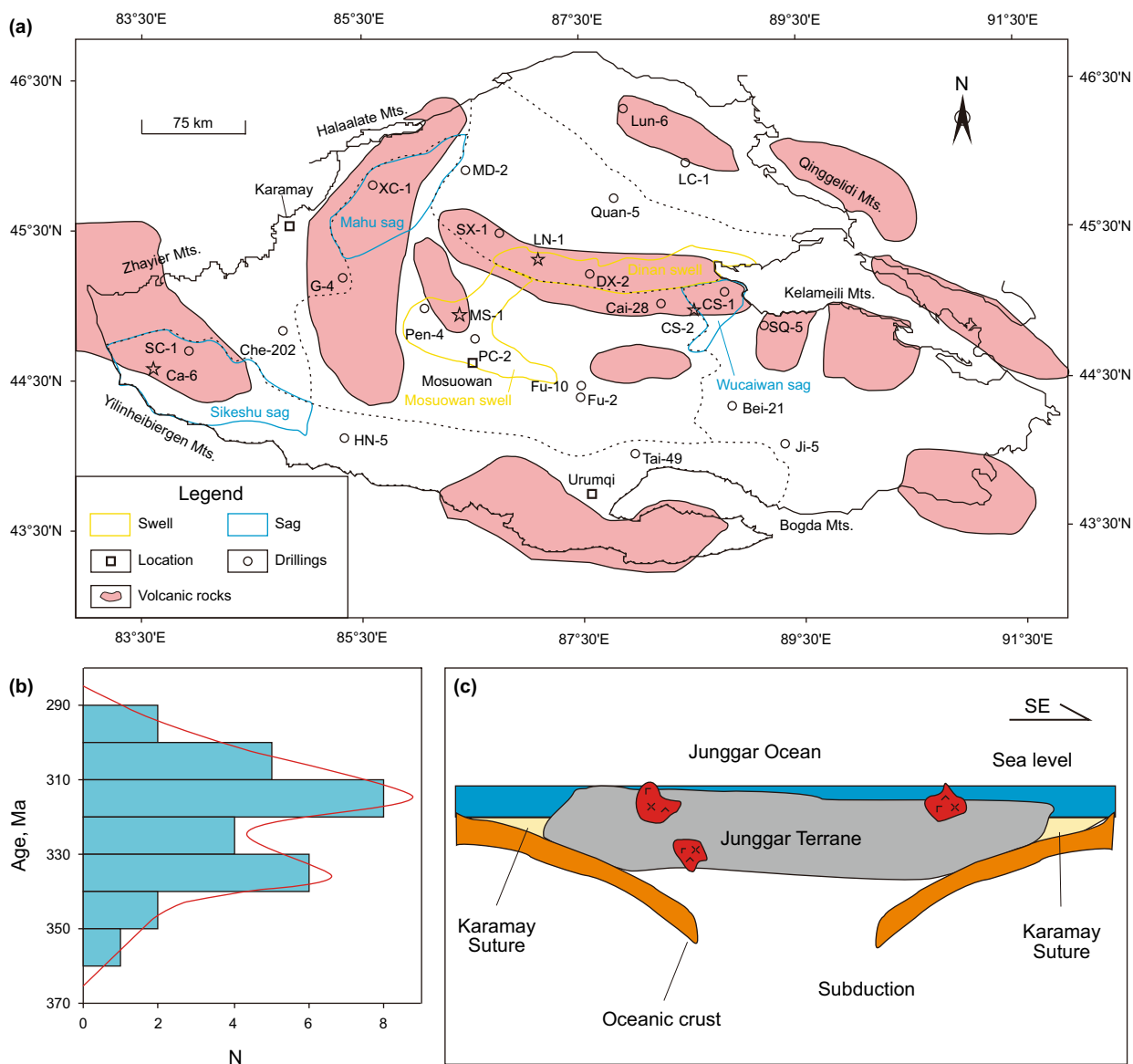


Fig. 9 Thermal maturity histories of Carboniferous source rocks for wells LN-1, MS-1, CS-2 and Ca-6

### 6 Conclusions

The thermal history of the Junggar Basin is quantitatively restored by integrating the paleo-geothermal gradient and paleo-heat flow methods constrained by considerable vitrinite reflectance data. Furthermore, the thermal maturation states of the Carboniferous source rocks for typical wells are



**Fig. 10** **a** The distribution of Carboniferous volcanic rocks (He et al. 2010). **b** Age distribution of igneous rocks and **c** geodynamic model of the Junggar Basin during the Carboniferous. Ages of igneous rocks are from Zheng et al. (2007), Tan et al. (2009), Yang et al. (2012b), Li et al. (2015) and Li et al. (2016)

identified based on 1D basin modeling. The following two major conclusions can be derived:

1. The paleo-heat flow of Junggar Basin was relatively high at ca. 80–120 mW/m<sup>2</sup> during the Carboniferous and Early Permian, which could be attributed to intense plate subduction and simultaneous large-scale volcanic activity. Meanwhile, considerable erosion is well documented in the Junggar Basin during this time. Later, the heat flow decreased rapidly during the Mesozoic and reached the present level of 40–60 mW/m<sup>2</sup> by the Cenozoic.
2. The source rocks of the Carboniferous started to generate hydrocarbons in the Late Carboniferous and are

characterized by rapid hydrocarbon maturation. Not only could the kerogen rapidly break through the dry gas period so that cracking of gas occurred, but it could also remain in the oil maturation window and form oil reservoirs based on the differences between the tectonic units and the depositional environments. Hence, from the perspective of thermal evolution, the Carboniferous source rocks have the potential to develop abundant hydrocarbon resources.

**Acknowledgements** This work was supported by the National Natural Science Foundation of China (No. 41502236 and 41877210) and the



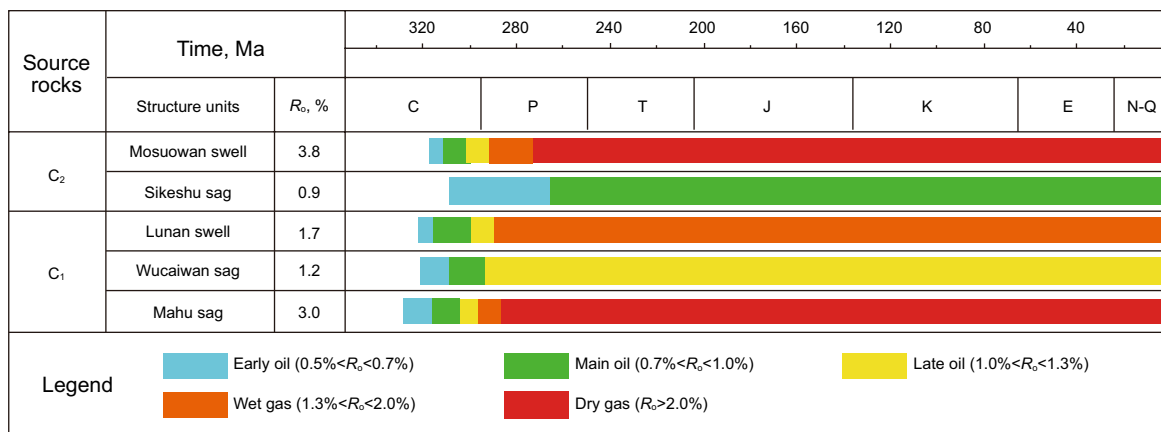


Fig. 11 Hydrocarbon maturation styles of deep Carboniferous source rocks in the Junggar Basin

National Foundation for Science and Technology Development (No. 2017ZX05008-004). The authors are very grateful to the PetroChina Xinjiang Oilfield Company for their kind help with lots of basic geological data; Dr. Guangzheng Jiang and Dr. Yibo Wang for discussion; Dr. Yizuo Shi for polishing the English. The authors also thank Associate Editor Jian Cao and all of the anonymous reviewers for their careful and useful comments that improved the revised manuscript.

**Open Access** This article is licensed under a Creative Commons Attribution 4.0 International License, which permits use, sharing, adaptation, distribution and reproduction in any medium or format, as long as you give appropriate credit to the original author(s) and the source, provide a link to the Creative Commons licence, and indicate if changes were made. The images or other third party material in this article are included in the article’s Creative Commons licence, unless indicated otherwise in a credit line to the material. If material is not included in the article’s Creative Commons licence and your intended use is not permitted by statutory regulation or exceeds the permitted use, you will need to obtain permission directly from the copyright holder. To view a copy of this licence, visit <http://creativecommons.org/licenses/by/4.0/>.

**References**

Cai XY. Overpressure development and oil charging in the central Junggar Basin, Northwest China: implication for petroleum exploration. *Sci China Ser D-Earth Sci.* 2009;52:1791–802. <https://doi.org/10.1007/s11430-009-0188-7>.

Cao J, Zhang Y, Hu W, et al. The Permian hybrid petroleum system in the northwest margin of the Junggar Basin, Northwest China. *Mar Pet Geol.* 2005;22(3):331–49. <https://doi.org/10.1016/j.marpetgeo.2005.01.005>.

Carroll AR, Graham SA, Smith ME. Walled sedimentary basins of China. *Basin Res.* 2010;22(1):17–32. <https://doi.org/10.1111/j.1365-2117.2009.00458.x>.

Chang J, Qiu N, Liu Y, et al. Maturity evolution of the carboniferous source rocks (CSR) in the Tarim Basin, Northwest China. *Sci Geol Sin.* 2014;49(3):823–41 (in Chinese with English abstract).

Chang J, Qiu N, Song X, et al. Multiple cooling episodes in the Central Tarim (Northwest China) revealed by apatite fission track analysis and vitrinite reflectance data. *Int J Earth Sci.* 2016;105:1257–72. <https://doi.org/10.1007/s00531-015-1242-7>.

Chang J, Qiu N, Xu W. Thermal regime of the Tarim Basin, Northwest China: a review. *Int Geol Rev.* 2017;59(1):45–61. <https://doi.org/10.1080/00206814.2016.1210546>.

Chang J, Qiu N, Zhao X, et al. Mesozoic and Cenozoic tectono-thermal reconstruction of the western Bohai Bay Basin (East China) with implications for hydrocarbon generation and migration. *J Asian Earth Sci.* 2018;160:380–95. <https://doi.org/10.1016/j.jseas.2017.09.008>.

Han BF, Guo ZJ, Zhang ZC, et al. Age, geochemistry, and tectonic implications of a late Paleozoic stitching pluton in the North Tian Shan suture zone, western China. *Geol Soc Am Bull.* 2010;122(3–4):627–40. <https://doi.org/10.1130/B26491.1>.

He DF, Chen XF, Kuang J, et al. Distribution of Carboniferous source rocks and petroleum systems in the Junggar Basin. *Pet Explor Dev.* 2010;37(4):397–408. [https://doi.org/10.1016/S1876-3804\(10\)60041-9](https://doi.org/10.1016/S1876-3804(10)60041-9).

He DF, Li D, Fan C, et al. Geochronology, geochemistry and tectonostratigraphy of Carboniferous strata of the deepest Well Moshen-1 in the Junggar Basin, northwest China: insights into the continental growth of Central Asia. *Gondwana Res.* 2013;24(2):560–77. <https://doi.org/10.1016/j.gr.2012.10.015>.

He ZL, Jin XH, Wo YJ, et al. Hydrocarbon accumulation characteristics and exploration domains of ultradeep marine carbonates in China. *China Pet Explor.* 2016;20(1):3–14 (in Chinese with English abstract).

Hu S, O’Sullivan PB, Raza A, et al. Thermal history and tectonic subsidence of the Bohai Basin, northern China: a Cenozoic rifted and local pull-apart basin. *Phys Earth Planet Inter.* 2001;126(3–4):221–35. [https://doi.org/10.1016/S0031-9201\(01\)00257-6](https://doi.org/10.1016/S0031-9201(01)00257-6).

Hudson SM, Hanson AD. Thermal maturation and hydrocarbon migration within La Popa Basin, Northeastern Mexico, with implications for other salt structures. *AAPG Bull.* 2010;94(3):273–91. <https://doi.org/10.1306/07130907012>.

Jin Z, Cao J, Hu W, et al. Episodic petroleum fluid migration in fault zones of the northwestern Junggar Basin (northwest China): evidence from hydrocarbon-bearing zoned calcite cement. *AAPG Bull.* 2008;92(9):1225–43. <https://doi.org/10.1306/06050807124>.

Jolivet M, Dominguez S, Charreau J, et al. Mesozoic and Cenozoic tectonic history of the central Chinese Tian Shan: reactivated tectonic structures and active deformation. *Tectonics.* 2010;29(6):1–70. <https://doi.org/10.1029/2010TC002712>.

Lerche I, Yarzab R, Kendall CSC. Determination of paleoheat flux from vitrinite reflectance data. *AAPG Bull.* 1984;68(11):1704–17. <https://doi.org/10.1007/BF01081374>.

- Li D, He D, Lian Y, et al. Structural evolution and late Carboniferous magmatism of the Zhongguai arc in the western Junggar Basin, Northwest China: implications for tectonic evolution of the Junggar Ocean. *Int Geol Rev.* 2016;59(10):1234–55. <https://doi.org/10.1080/00206814.2016.1160801>.
- Li D, He D, Santosh M, et al. Tectonic framework of the northern Junggar Basin part I: the eastern Luliang Uplift and its link with the East Junggar terrane. *Gondwana Res.* 2015;27(3):1089–109. <https://doi.org/10.1016/j.gr.2014.08.015>.
- Li J, Jiang Z, Xia L, et al. Geochemical characteristics of coal-measure source rocks and coal-derived gas in Junggar Basin, NW China. *Pet Explor Dev.* 2009;36(3):1365–74. [https://doi.org/10.1016/S1876-3804\(09\)60133-6](https://doi.org/10.1016/S1876-3804(09)60133-6).
- Luo X, Wang Z, Zhang L, et al. Overpressure generation and evolution in a compressional tectonic setting, the southern margin of Junggar Basin, northwestern China. *AAPG Bull.* 2007;91(8):1123–39. <https://doi.org/10.1306/02260706035>.
- Ma WJ, Wei YZ, Tao SZ. A method for evaluating paleo hydrocarbon pools and predicting secondary reservoirs: a case study of the Sangonghe Formation in the Mosuowan area, Junggar Basin. *Pet Sci.* 2018;15(2):252–69. <https://doi.org/10.1007/s12182-018-0231-4>.
- Mashhadi ZS, Rabbani AR, Kamali MR, et al. Burial and thermal maturity modeling of the Middle Cretaceous-Early Miocene petroleum system, Iranian sector of the Persian Gulf. *Pet Sci.* 2015;12(3):367–90. <https://doi.org/10.1007/s12182-015-0040-y>.
- Pan C, Zhou Z, Fan S, et al. Thermal history of Junggar basin. *Geochim.* 1997;26(6):1–7 (in Chinese with English abstract).
- Qiu N, Zha M, Wang X, et al. Tectono-thermal evolution of the Junggar Basin, NW China: constraints from R<sub>o</sub> and apatite fission track modelling. *Pet Geosci.* 2005;11(4):361–72. <https://doi.org/10.1144/1354-079304-655>.
- Qiu N, Zhang Z, Xu E. Geothermal regime and Jurassic source rock maturity of the Junggar basin, northwest China. *J Asian Earth Sci.* 2008;31(4–6):464–78. <https://doi.org/10.1016/j.jseas.2007.08.001>.
- Qiu N, Chang J, Zuo Y, Wang J, Li H. Thermal evolution and maturation of lower Paleozoic source rocks in the Tarim Basin, northwest China. *AAPG Bull.* 2012;96(5):789–821. <https://doi.org/10.1306/09071111029>.
- Rao S, Hu S, Zhu C, et al. The characteristics of heat flow and lithospheric thermal structure in Junggar Basin, northwest China. *Chin J Geophys.* 2013;56:2760–70. <https://doi.org/10.6038/cjg20130824> (in Chinese with English abstract).
- Şengör A, Natal'In B, Burtman V. Evolution of the Altai tectonic collage and Palaeozoic crustal growth in Eurasia. *Nature.* 1993;364(6435):299–307. <https://doi.org/10.1038/364299a0>.
- Sun L, Zou C, Zhu R, et al. Formation, distribution and potential of deep hydrocarbon resources in China. *Pet Explor Dev.* 2013;40(6):687–95. [https://doi.org/10.1016/S1876-3804\(13\)60093-2](https://doi.org/10.1016/S1876-3804(13)60093-2).
- Sweeney JJ, Burnham AK. Evaluation of a simple model of vitrinite reflectance based on Chemical kinetics. *AAPG Bull.* 1990;74(10):1559–70.
- Tan J, Wu R, Zhang Y, et al. Characteristics and geochronology of volcanic rocks of Batamayineishan Formation in Kalamaili, Eastern Junggar, Xinjiang. *Acta Pet Sin.* 2009;25(3):539–46. <https://doi.org/10.1016/j.sedgeo.2009.01.006>.
- Tang X, Yang S, Hu S. Thermal and maturation history of Jurassic source rocks in the Kuqa foreland depression of Tarim Basin, NW China. *J Asian Earth Sci.* 2014;89(5):1–9. <https://doi.org/10.1016/j.jseas.2014.03.023>.
- Wang S, He L, Wang J. Thermal regime and petroleum systems in Junggar basin, northwest China. *Phys Earth Planet Inter.* 2001;126(3–4):237–48. [https://doi.org/10.1016/s0031-9201\(01\)00258-8](https://doi.org/10.1016/s0031-9201(01)00258-8).
- Wang X, Zhao M, Xiang B, et al. Carboniferous source rocks in the Ludong-Wucuiwan area, Junggar Basin, NW China. *Pet Explor Dev.* 2010;37(5):523–30. [https://doi.org/10.1016/s1876-3804\(10\)60052-3](https://doi.org/10.1016/s1876-3804(10)60052-3).
- Wang XL, Zhong DM, Wang YT, et al. Geochemistry of source rock and petroleum in the Junggar Basin. Beijing: Petroleum Industry Press; 2013. p. 1–565 (in Chinese).
- Xiao W, Han C, Yuan C, et al. Middle Cambrian to Permian subduction-related accretionary orogenesis of Northern Xinjiang, NW China: implications for the tectonic evolution of central Asia. *J Asian Earth Sci.* 2008;32(2):102–17. <https://doi.org/10.1016/j.jseas.2007.10.008>.
- Xiao Y, Zhang H, Shi JA, et al. Late Paleozoic magmatic record of East Junggar, NW China and its significance: implication from zircon U-Pb dating and Hf isotope. *Gondwana Res.* 2011;20(2–3):532–42. <https://doi.org/10.1016/j.gr.2010.12.008>.
- Xu Y, Chung SL, Jahn BM, et al. Petrologic and geochemical constraints on the petrogenesis of Permian-Triassic Emeishan flood basalts in southwestern China. *Lithos.* 2001;58(3–4):145–68. [https://doi.org/10.1016/S0024-4937\(01\)00055-X](https://doi.org/10.1016/S0024-4937(01)00055-X).
- Xu YG, Wei X, Luo ZY, et al. The Early Permian Tarim Large Igneous Province: main characteristics and a plume incubation model. *Lithos.* 2014;204(1):20–35. <https://doi.org/10.1016/j.litho.2014.02.015>.
- Yang XF, He DF, Wang QC, et al. Tectonostratigraphic evolution of the Carboniferous arc-related basin in the East Junggar Basin, northwest China: insights into its link with the subduction process. *Gondwana Res.* 2012a;22(3–4):1030–46. <https://doi.org/10.1016/j.gr.2012.02.009>.
- Yang XF, He DF, Wang QC, et al. Provenance and tectonic setting of the Carboniferous sedimentary rocks of the East Junggar Basin, China: evidence from geochemistry and U-Pb zircon geochronology. *Gondwana Res.* 2012b;22(2):567–84. <https://doi.org/10.1016/j.gr.2011.11.001>.
- Yu S, Wang X, Xiang B, et al. Organic geochemistry of Carboniferous source rocks and their generated oils from the Eastern Junggar Basin, NW China. *Organ Geochem.* 2014;77:72–88. <https://doi.org/10.1016/j.orggeochem.2014.09.011>.
- Zhang SC, Liang DG, Zhu GY, et al. Fundamental geological elements for the occurrence of Chinese marine oil and gas accumulations. *Sci Bull.* 2007;52(1):28–43. <https://doi.org/10.1007/s11434-007-6020-x>.
- Zhang Z, Zhou G, Kusky TM, et al. Late Paleozoic volcanic record of the Eastern Junggar terrane, Xinjiang, Northwestern China: major and trace element characteristics, Sr–Nd isotopic systematics and implications for tectonic evolution. *Gondwana Res.* 2009;16(2):201–15. <https://doi.org/10.1016/j.gr.2009.03.004>.
- Zhao X, Jin Q, Jin F, et al. Origin and accumulation of high-maturity oil and gas in deep parts of the Baxian Depression, Bohai Bay Basin, China. *Pet Sci.* 2013;10(3):303–13. <https://doi.org/10.1007/s12182-013-0279-0>.
- Zheng J, Sun M, Zhao G, et al. Elemental and Sr–Nd–Pb isotopic geochemistry of Late Paleozoic volcanic rocks beneath the Junggar basin, NW China: implications for the formation and evolution of the basin basement. *J Asian Earth Sci.* 2007;29(5–6):778–94. <https://doi.org/10.1016/j.jseas.2006.05.0041>.
- Zhu CQ, Ming X, Yuan YS, et al. Palaeogeothermal response and record of the effusing of Emeishan basalts in the Sichuan basin. *Sci Bull.* 2010;55(10):949–56. <https://doi.org/10.1007/s11434-009-0490-y>.